

# A FINITE ELEMENT MODEL FOR 3D PRINTED RECYCLED PARTS FROM END-OF-LIFE WIND TURBINE BLADES

Yan Z<sup>1</sup>\*, Rahimizadeh A<sup>1</sup>, Zhang Y<sup>1</sup>, and Lessard L<sup>1</sup>

<sup>1</sup> Department of Mechanical Engineering, McGill University, Montreal, Canada

\* Corresponding author (zhengshu.yan@mail.mcgill.ca)

**Keywords:** *Wind turbine blades, Fused filament fabrication, Representative volume element*

## ABSTRACT

Wind turbines are important for clean electric energy, but the increasing number of end-of-life wind turbine blades has become a hazardous waste problem worldwide. A novel recycling approach based on mechanical grinding and combined with 3D printing techniques is a promising solution that will reduce waste at a low cost while retaining the excellent mechanical properties of recycled fabricated samples.

Considering the material structure complexity of 3D printed material samples, the Representative Volume Element (RVE) stands out among many predictive simulation models. This paper proposes a Modified Random Sequential Adsorption (MRSA) algorithm for the efficient generation of the RVEs with hybrid and arbitrary-geometry reinforcements. Compared with the classical RSA algorithm, MRSA shows excellent advantages in computational cost in determining fiber intersection. The error between FEA and experimental data is lower than the results obtained from Mori-Tanaka and Halpin-Tsai. The effects of fiber content, fiber aspect ratio, fiber orientation, fiber density etc., are discussed. The model will be helpful for accurately predicting the results of using recycled wind turbine materials in the field of 3D printing.

## 1 INTRODUCTION

### 1.1 Recycling background

Although wind energy is a good choice for sustainable energy production, the overwhelming use of composite wind turbine blades and the accelerating growth of the wind energy industry has caused significant quantities of material waste and undesirable environmental impacts [1, 2]. Although 85% of wind turbines (like housing and tower parts) are made of recyclable materials like copper and steel [3], non-biodegradable materials such as fiberglass, plastic polymer, and core are used to build high-performance wind turbine blades and enhance their efficiency [4]. Turbine blades have a life span of 25 years, and many of the initial generations of turbines are already reaching their end-of-life. Therefore, wind turbine blades have become a significant primary source of composite waste generation [2]. It is predicted that the annual amount of waste from end-of-life wind turbine blades will increase from over 50,000 tonnes in 2021 to over 200,000 tonnes worldwide by 2034 [5].

Compared with the common recycling routes like landfill and incineration, mechanical grinding has considerable advantages since it is straightforward, environmental-friendly, and economically feasible. Moreover, the size of composite waste particles can be efficiently reduced by mechanical grinding due to the abrasive nature of glass fibers [6]. This technique reduces the size of scrap composites by size reduction processes that include shredding, milling, grinding, etc., and reconstitutes them as reinforcement into new composite structures [6-10].

To address the blade waste problem, Rahimizadeh et al. [11] proposed a recycling solution based on mechanical grinding and the fused filament fabrication (FFF) 3D printing technique as a solution for end-of-life glass fiber reinforced wind turbine blades (Figure 1). The solution entails a detailed step-by-step process that results in structurally stiff and strong recycled parts. Specifically, discontinuous short and long glass fibers covered in epoxy residue from end-of-life scrap wind turbine blades are reclaimed. They are incorporated into an extrusion process mixed with polylactic acid (PLA) to generate fiber-reinforced filaments with enhanced mechanical properties (Figure 2). The filament is then used as feedstock for FFF 3D printing applications.



Figure 1. The recycling schemes of mechanical grinding and FFF 3D printing [11].

Rahimizadeh et al. [11] carried out several mechanical tests to assess the mechanical performance of the newly introduced recycled parts. The results demonstrated a promising recycling solution for end-of-life wind turbine blades with mechanical performance enhancement and no adverse environmental impact. Specifically, compared with pure thermoplastic feedstock materials on the market, this newly developed feedstock offers up to 20% and 28% enhancement in tensile strength and stiffness, respectively.

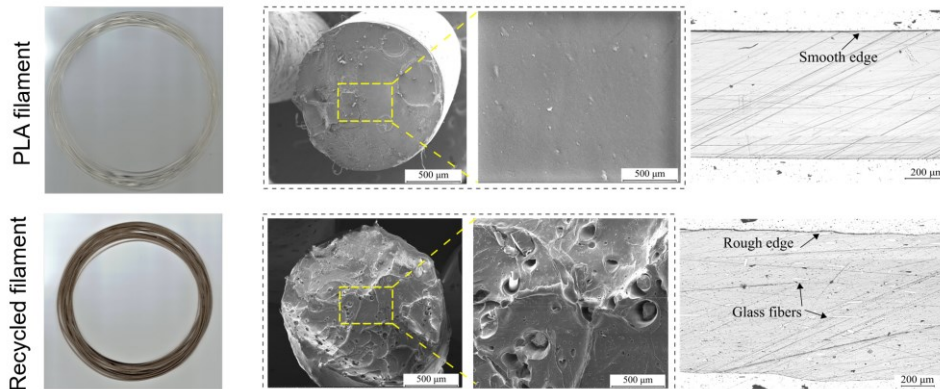


Figure 2. Pure PLA, recycled filaments, and corresponding scanning electron microscope (SEM) images [11].

### 1.2 Numerical simulations

Simulation models like numerical models, finite element analysis (FEA) models, etc., are necessary to facilitate the design process and material assessment in the currently proposed recycling solution. Numerical models are helpful because the methods are well-studied, and there are no restrictions on the composite's geometry, material

properties, and phase angles [12]. Among all available numerical models, the work of Mori and Tanaka is well-known [13]. For the discontinuous random fiber reinforcement composites manufactured from this recycling solution, the material behaviour and performance are affected by several factors: fiber aspect ratio, fiber orientation, reinforcement shape, etc. [14-16]. Moreover, other factors, like voids and particles, reduce the accuracy of numerical models. In this sense, finite element analysis (FEA) can provide appealing alternatives, but only if they include all pertinent aspects of the problem.

Explicit modelling of a 3D printed composite component with all the features can be computationally prohibitive. Enormous computational resources and impracticalities are required to obtain a convergent solution. To overcome this hurdle, mechanical analysis methods can be beneficial to obtain the effective mechanical properties of the material via analyzing a representative volume element (RVE) [17]. An RVE must be sufficiently large to include enough reinforcements. In addition, the effective properties of the RVE must statistically represent the actual material properties on a macroscopic scale [18]. At the same time, choosing a larger size of RVE comes with a higher computational cost. Therefore, the size of RVE should be minimized for computational efficiency but must guarantee accuracy.

The RVE must have identical fiber volume fraction and elastic constants as the original composite. As illustrated in Figure 3, the macrostructure of a 3D printed sample can be represented through 3 orders of hierarchy, including the extrudates, 3D printing building block incorporating interlayer voids, and composite compound unit.

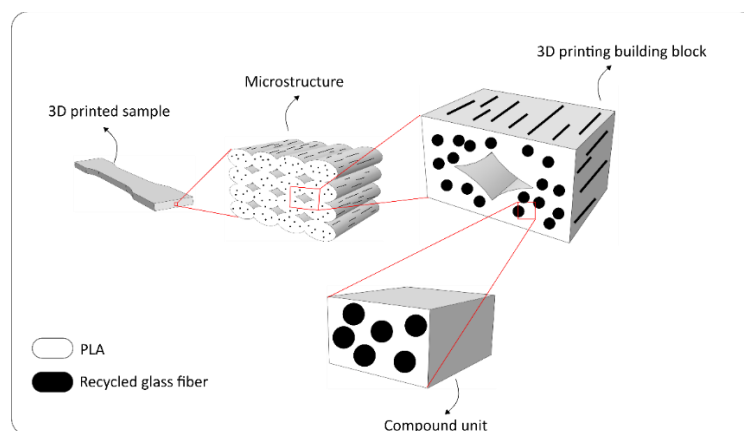


Figure 3. The 3-order hierarchical structure of a 3D printed sample.

## 2 MICROMECHANICAL FE ANALYSIS

### 2.1 Generation of RVEs

Essential to the FE analysis, three basic notions enable the prediction of elastic properties of recycled 3D printed parts: (1) The creation of distinct hierarchical orders that represent the macrostructure of 3D printed parts; (2) the evaluation of elastic properties of randomly distributed fibers within a cubic RVE via the homogenization method; and (3) the assessment of structural stiffness and Poisson's ratios of 3D printed parts via formulating the homogenization problem on the 3D printing building block.

### 2.1.1 Generation of RVE cuboid

The RVE cubic volume is considered first, which has been assigned a size obtained through a sensitivity analysis and comparison with experimental data. Previous relevant studies are also referred to, which suggest that the length of RVE needs to be at least twice the average length of fibers to achieve satisfactory results [19]. Note that this conclusion was stated for the case that all fibers lengths are identical, which is not the case for the current recycling method. The length of fibers is essential in terms of average length and fiber length distribution.

### 2.1.2 Generation of fibers

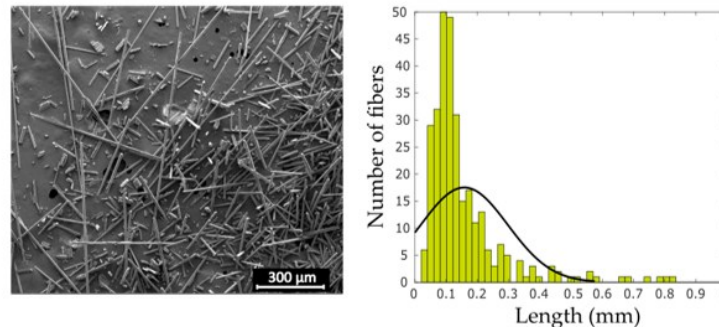


Figure 4. SEM image of fibers and fiber length distribution [11, 20].

The fibers are modelled as straight cylinders with circular cross-sections of a constant radius. This is due to small aspect ratios, low volume fraction [19], and the fact that a non-constant radius of fibers would have an insignificant effect on the elastic properties [21]. The constant radius is set as the mean value of the actual fiber radius measured from experiments, and the length range of fibers is obtained following the classification operation (Figure 4).

Several variables are required to describe the state of fibers in the RVE cuboid, namely, the fibers' position conferred by a random function, the length selected from the length range of recycled fibers, the radius, and two orientation angles. The fiber orientations are divided into two groups, namely the unidirectional (UD) group and the randomly directional (RD) group, since in experiments, most fibers are predominantly oriented in one direction, and relatively fewer are aligned in random directions (Figure 5). Furthermore, there can be no intersection between fibers within the RVE frame since it is physically unacceptable. The periodicity of the geometry is ensured by translating fiber parts that penetrate the exterior surface of the RVE frame to the opposite side (face) inside the RVE frame.

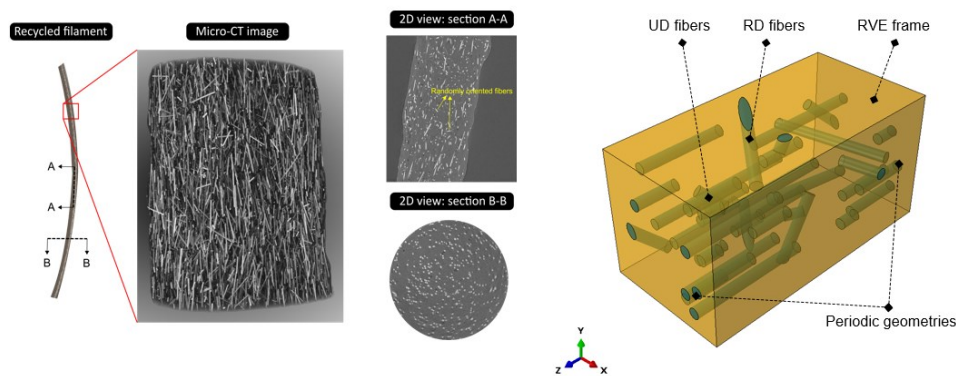


Figure 5. The micro-computed tomography (CT) scan of recycled filament and corresponding RVE.

The generation of the fibers is realized through a modified random sequential adsorption (MRSA) algorithm by using ABAQUS CAE and PYTHON scripts. The algorithm avoids redundant calculations in checking the violation of the fiber intersections compared to the classic RSA algorithms. In the classical RSA algorithm, each newly generated candidate fiber needs to be tested with all previously accepted fibers. In the proposed new MRSA algorithm, only one bulk calculation is required (Figure 6). Moreover, another crucial advance is that the algorithm relieves the limitation of the generation for arbitrary geometries and has fewer misjudgments in some particular cases (e.g., one fiber end is nearly in contact with another fiber).

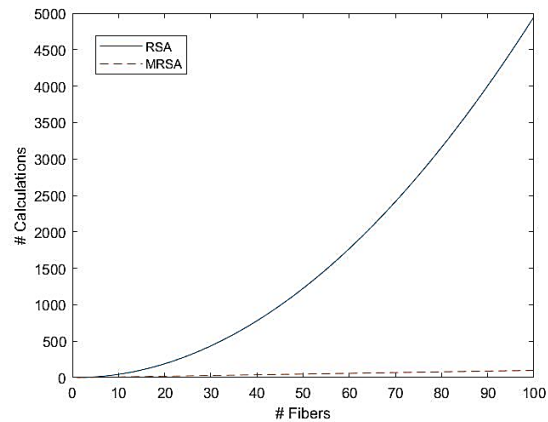


Figure 6. Number of calculations required for RSA and MRSA to judge possible fiber intersections.

## 2.2 Homogenization

The algorithm will continue until the desired RVE is attained (Figure 7). The data of reinforcement states are then exported to rebuild, mesh, and solve the 3D problem of randomly distributed recycled fiber composites, modelled with 10-node quadratic tetrahedron elements (C3D10). PBC with non-periodic meshes is imposed by using an interpolation technique, which is implanted into the plugin tool EasyPBC [22].

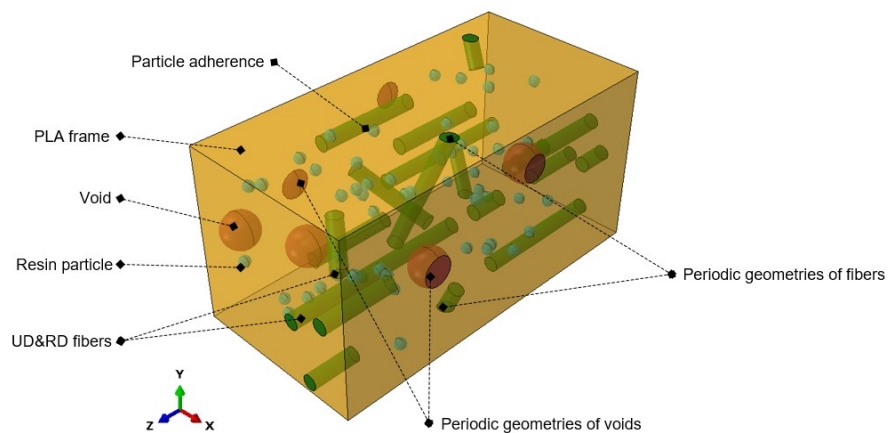


Figure 7. RVE hierarchical structure of recycled glass fiber reinforced extrudate.

### 3 RESULTS AND DISCUSSION

The procedures described in this work are used for the FE analysis of 3D printed recycled composite parts made from PLA and recycled glass fibers. The properties of the fibers adopted here are obtained from a single fiber tensile test on fiber extracted from the ground used wind turbine blades [23]. As a result, the matrix and fibers were assigned Young's modulus and Poisson's ratio of, respectively,  $E_m = 3.6$  GPa,  $\nu_m = 0.33$ ;  $E_f = 75$  GPa,  $\nu_f = 0.22$ . The actual fiber content of the filaments obtained via Thermogravimetric Analysis (TGA) was used to predict the mechanical properties of the parts using FE and mechanical theories of short fiber composites. The effects of fibers, fiber distributions, voids and resin particles were studied.

#### 3.1 Effects of fiber content

Glass fibers play a decisive role in the mechanical performance of the part since fibers occupy the most significant proportion relative to other inclusions like resin particles and voids. The mechanical properties of 3D printed specimens with three different fiber contents, including 0, 5, and 10 wt%, are predicted. The numerical results and the experimental data are shown in Figure 8.

The stiffness in the direction of the leading fiber distribution (3-direction) is one of the most important design parameters. This stiffness obtained by FE and micromechanical models is quantitatively in good agreement with the measurements reproducing the key trends observed in the experiments. The results offer a better prediction than analytical models like Mori-Tanaka and Halpin-Tsai since the realistic model details from this RVE model effectively reduce errors with the experimental results. However, it still shows an overestimation between the FE results and the experimental measurements at all the fiber contents. These results indicate proper minimization of intrinsic and extrinsic defects and voids, the leading cause of property degradation in these short fiber samples.

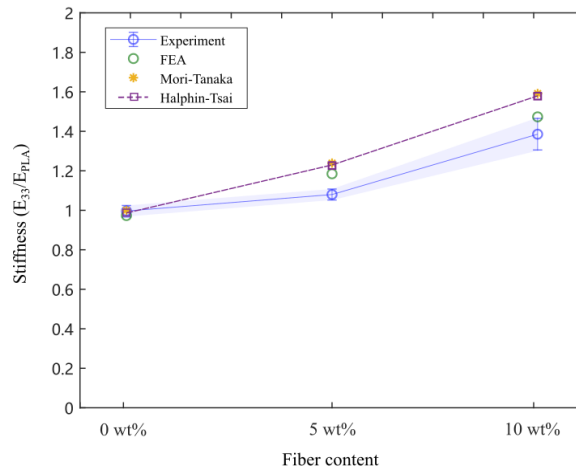


Figure 8. Normalized stiffness of 3D printed specimens from FE, analytical, and experiments.

In addition to stiffness, an increase in the fiber content also changes the average fiber aspect ratio and the Poisson's ratios of the RVE (Figure 9), which will, in turn, affect the properties of the printed specimens. This phenomenon occurs because longer fibers are more likely to be selected in a higher fiber content generation when the fiber radius is constant. Meanwhile,  $\nu_{12}$  and  $\nu_{21}$  rise steadily due to the constraining effect, i.e., the matrix is constrained to stay on the fibers, leading to bigger Poisson's ratios. Other Poisson's ratios decline, especially  $\nu_{13}$  and  $\nu_{23}$  suffer a dramatic drop because there are more fibers overall (mainly in the 3-direction) which affects the size of these Poisson's terms.

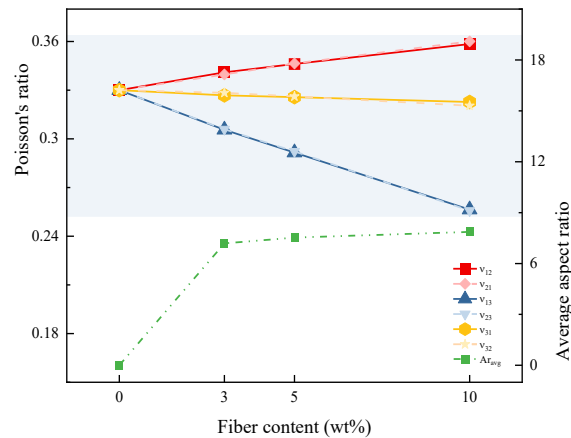


Figure 9. Poisson's ratios and average aspect ratios versus fiber content for 3D printed specimens.

### 3.2 Effects of fiber aspect ratio

For the same fiber content, stiffness and Poisson's ratios vary due to the variations in fiber aspect ratios. As shown in Figure 10, for each set of fiber content, an upward trend in the stiffness can be witnessed in each data set as the average fiber aspect ratio goes up. All coefficients of determination ( $R^2$ ) are over 0.88, which fully indicates a linear correlation. It is noteworthy that some of the results are above the trendline due to the existence of RD fibers. When the orientations of some large fibers are not incorporated as unidirectional, the stiffness in the 3-direction will be relatively lower. However, the stiffness in the 3-direction is still positively correlated with the average fiber aspect ratio due to the dominance of UD fibers. The effect of UD fibers can also be verified because the growth rate of stiffness in the 10 wt% fiber group is higher than in the other two groups, i.e., the linear trendline has an increasing slope with fiber content.

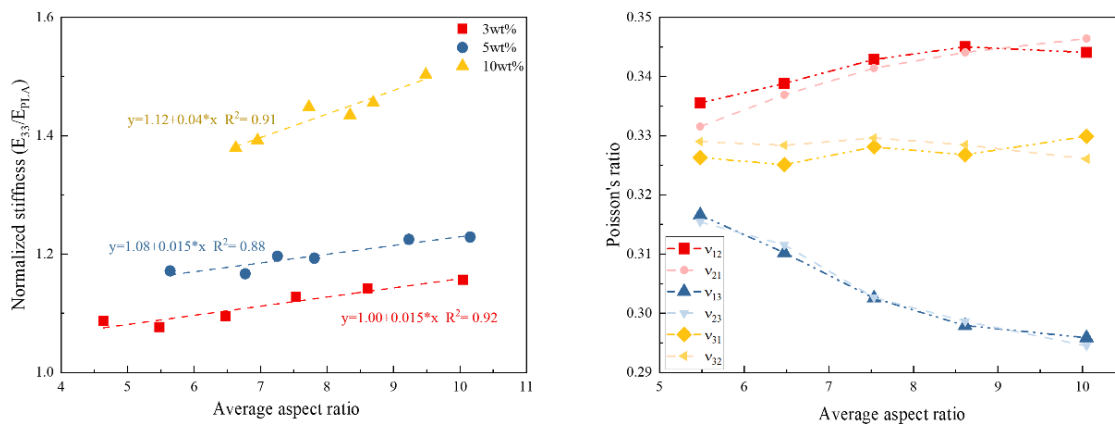


Figure 10. Normalized stiffness and Poisson's ratio versus average fiber aspect ratio.

Two Poisson's ratios ( $v_{13}$  and  $v_{23}$ ) considerably decrease while other ratios fluctuate when the average aspect ratio changes and fiber content remains the same (Figure 10). When fiber content is no longer the critical factor, RD fibers will disrupt the consistency of the change of Poisson's ratios in the 1-direction and the 2-direction.  $v_{13}$  and  $v_{23}$  are not much affected by this disturbance because the 3-direction is the direction with the most fibers.

### 3.3 Effect of fiber orientation

As a result of the typical filament-making process, most fibers are unidirectionally oriented in the extrudate direction (3-direction), while others are arranged in random directions. This phenomenon seems to overshadow the possibility of the 3D printed specimen being an orthotropic-like short-fiber composite. To analyze the effects of fiber orientation, especially the effects of RD fibers, four models with the same fiber content but different packings are examined: (a) Center packing: a single fiber at center of RVE; (b) Quarter packing: a single fiber at RVE center plus four fiber quarters at RVE corner; (c) Transverse packing: all fibers aligned in the 3-direction in RVE; and (d) Random packing: RVE packing (Figure 11).

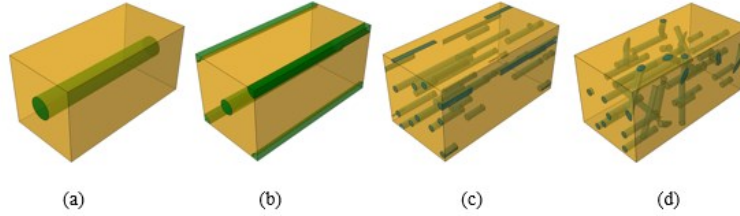


Figure 11. Fiber packings with the same fiber volume content: (a) Central; (b) Quarter; (c) Transverse; and (d) Random.

The normalized stiffness and Poisson's ratios ( $\nu_{31}$  and  $\nu_{32}$ ) of samples featuring four different fiber contents, including 0 wt%, 3 wt%, 5 wt% and 10 wt%, are obtained from FE analysis to explore the orthotropy of the 3D printed specimens (Figure 12). The average of  $\nu_{31}$  and  $\nu_{32}$  are taken for Random packing since they are close. When setting the experimental results as a baseline, the Random packing seems to be the most realistic representation of 3D printed specimens because it is the closest to the experimental data. Transverse packing is appropriate for stiffness but is not suitable for characterizing Poisson's ratios because the low average fiber aspect ratio and fiber alignment in the same direction leads to higher Poisson's ratios. The other two packings are even more inaccurate. Therefore, the RD fibers have a pronounced influence on material behaviour that cannot be neglected. Furthermore, the random occurrences of voids and particles make the distribution of reinforcements more disorderly.

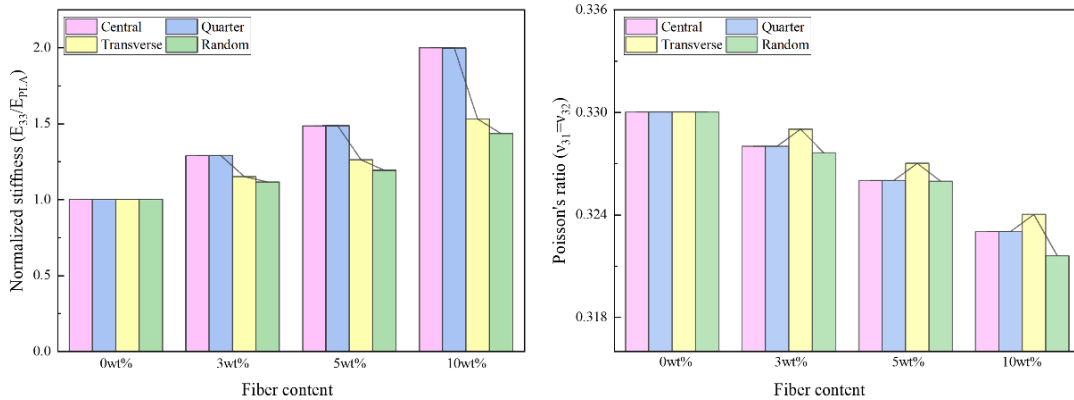


Figure 12. Normalized stiffness and Poisson's ratio versus fiber content.

### 3.4 Effects of fiber center-concentration

It is observed that fibers tend to be concentrated to some extent in the center of the filament that is used to make the 3D printed specimens. Thus, the effect of fiber density distribution within the RVE frame is also studied. A new variable, termed Fiber Center-Concentration Factor (CCF), is introduced to characterize the degree of fiber

convergence to the RVE center. For example, a CCF with 10% means all fibers are distributed in 90% of the volume area closest to the RVE center.

Stiffness in the 3-direction and the stiffness via Rule-of-Mixture (RoM) as per the proportions of UD and RD fibers are used to evaluate the influences of CCF. The effects of fiber CCF on the normalized stiffness of the 3D printed specimens are shown in Figure 13. As fibers converge toward the RVE center, the stiffness falls modestly at first since fewer fibers are located near the RVE boundary, thereby dividing local stress among fibers and the RVE boundary. When the fiber spacing is further reduced, local stress transfer among fibers dominates the overall RVE conditions, so the stiffness climbs significantly.

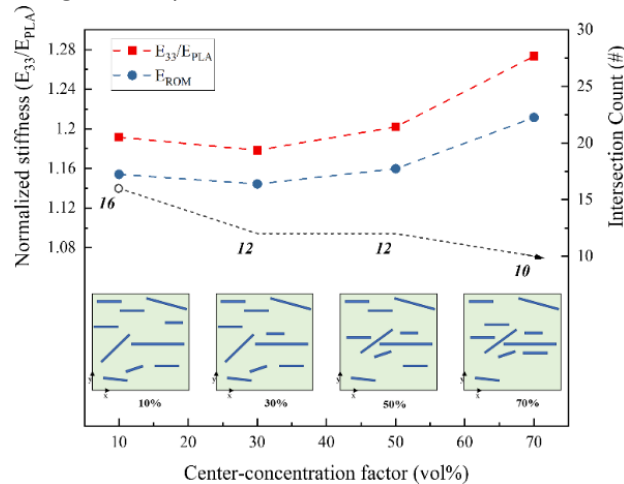


Figure 13. Effects of fiber CCF on normalized stiffness of the 3D printed specimen.

## 4 CONCLUSIONS

An RVE model for 3D printed recycled parts from end-of-life wind turbine blades is established in this work. An MRSA algorithm is built to enable the ease of efficiently generating RVEs with hybrid arbitrary-geometry reinforcements. A special boundary treatment is applied to impose the PBC without periodic meshes. FE analysis was performed, and the mechanical properties gained from 3D-printed recycled filaments were validated and discussed. This MRSA algorithm could also be combined with other well-built algorithms for some exceptional cases, such as an RVE with irregular geometric shapes of reinforcements or various reinforcements to integrate the advantages of different methods. The RVE model has great potential for helping to characterize and optimize the design of 3D-printed recycled filaments.

The main findings of the model: (1) Glass fiber content plays a dominant role in the material properties of filaments. (2) Fiber aspect ratio also affects the material properties of filaments. (3) Although only a small amount of randomly directional fibers is present in filaments, their influence on the material properties of filaments cannot be ignored. (4) The concentration of fibers towards the center in filaments impacts the material properties of filaments.

## 5 REFERENCES

- [1] J. Chen, J. Wang, and A. Ni, "Recycling and reuse of composite materials for wind turbine blades: An overview," *Journal of Reinforced Plastics and Composites*, vol. 38, no. 12, pp. 567-577, 2019.

- [2] D. S. Cousins, Y. Suzuki, R. E. Murray, J. R. Samaniuk, and A. P. Stebner, "Recycling glass fiber thermoplastic composites from wind turbine blades," *Journal of cleaner production*, vol. 209, pp. 1252-1263, 2019.
- [3] L. Mishnaevsky, K. Branner, H. N. Petersen, J. Beauson, M. McGugan, and B. F. Sorensen, "Materials for Wind Turbine Blades: An Overview," (in eng), *Materials (Basel)*, vol. 10, no. 11, Nov 9 2017, doi: 10.3390/ma10111285.
- [4] H. Albers, S. Greiner, H. Seifert, and U. Kühne, "Recycling of wind turbine rotor blades. Fact or fiction?; Recycling von Rotorblättern aus Windenergieanlagen. Fakt oder Fiktion?," *DEWI-Magazin*, 2009.
- [5] K. Larsen, "Recycling wind turbine blades," *Renewable energy focus*, vol. 9, no. 7, pp. 70-73, 2009.
- [6] S. A. Martin, "Comparison of hammermill and roller mill grinding and the effect of grain particle size on mixing and pelleting," 1985.
- [7] J. Palmer, O. R. Ghita, L. Savage, and K. E. Evans, "Successful closed-loop recycling of thermoset composites," *Composites Part A: Applied Science and Manufacturing*, vol. 40, no. 4, pp. 490-498, 2009.
- [8] G. Schinner, J. Brandt, and H. Richter, "Recycling carbon-fiber-reinforced thermoplastic composites," *Journal of Thermoplastic Composite Materials*, vol. 9, no. 3, pp. 239-245, 1996.
- [9] T. Inoh, T. Yokoi, K.-I. Sekiyama, N. Kawamura, and Y. Mishima, "SMC recycling technology," *Journal of Thermoplastic Composite Materials*, vol. 7, no. 1, pp. 42-55, 1994.
- [10] M. Roux, C. Dransfeld, N. Eguémann, and L. Giger, "Processing and recycling of a thermoplastic composite fibre/peek aerospace part," in *Proceedings of the 16th European conference on composite materials (ECCM 16)*, 2014, pp. 22-26.
- [11] A. Rahimizadeh, J. Kalman, K. Fayazbakhsh, and L. Lessard, "Recycling of fiberglass wind turbine blades into reinforced filaments for use in Additive Manufacturing," *Composites Part B*, vol. 175, 2019, doi: 10.1016/j.compositesb.2019.107101.
- [12] S. Kari, H. Berger, and U. Gabbert, "Numerical evaluation of effective material properties of randomly distributed short cylindrical fibre composites," *Computational Materials Science*, vol. 39, no. 1, pp. 198-204, 2007, doi: 10.1016/j.commatsci.2006.02.024.
- [13] T. Mori and K. Tanaka, "Average stress in matrix and average elastic energy of materials with misfitting inclusions," *Acta metallurgica*, vol. 21, no. 5, pp. 571-574, 1973.
- [14] B. D. Agarwal, L. J. Broutman, and K. Chandrashekhara, *Analysis and performance of fiber composites*. John Wiley & Sons, 2006.
- [15] L. T. Harper, T. A. Turner, N. A. Warrior, and C. D. Rudd, "Characterisation of random carbon fibre composites from a directed fibre preforming process: The effect of fibre length," *Composites Part A: Applied Science and Manufacturing*, vol. 37, no. 11, pp. 1863-1878, 2006, doi: 10.1016/j.compositesa.2005.12.028.
- [16] L. T. Harper, T. A. Turner, N. A. Warrior, and C. D. Rudd, "Characterisation of random carbon fibre composites from a directed fibre preforming process: The effect of tow filamentisation," *Composites Part A: Applied Science and Manufacturing*, vol. 38, no. 3, pp. 755-770, 2007, doi: 10.1016/j.compositesa.2006.09.008.
- [17] S. Arabnejad and D. Pasini, "Mechanical properties of lattice materials via asymptotic homogenization and comparison with alternative homogenization methods," *International Journal of Mechanical Sciences*, vol. 77, pp. 249-262, 2013.
- [18] R. Hill, "Elastic properties of reinforced solids: some theoretical principles," *Journal of the Mechanics and Physics of Solids*, vol. 11, no. 5, pp. 357-372, 1963.
- [19] W. Tian, L. Qi, J. Zhou, J. Liang, and Y. Ma, "Representative volume element for composites reinforced by spatially randomly distributed discontinuous fibers and its applications," *Composite Structures*, vol. 131, pp. 366-373, 2015, doi: 10.1016/j.compstruct.2015.05.014.
- [20] A. Rahimizadeh, J. Kalman, R. Henri, K. Fayazbakhsh, and L. Lessard, "Recycled Glass Fiber Composites from Wind Turbine Waste for 3D Printing Feedstock: Effects of Fiber Content and Interface on Mechanical Performance," *Materials*, vol. 12, no. 23, p. 3929, 2019. [Online]. Available: <https://www.mdpi.com/1996-1944/12/23/3929>.
- [21] A. A. Gusev, P. J. Hine, and I. M. Ward, "Fiber packing and elastic properties of a transversely random unidirectional glass/epoxy composite," *Composites Science and Technology*, vol. 60, no. 4, pp. 535-541, 2000.
- [22] S. L. Omairey, P. D. Dunning, and S. Sriramula, "Development of an ABAQUS plugin tool for periodic RVE homogenisation," *Engineering with Computers*, vol. 35, no. 2, pp. 567-577, 2019.
- [23] M. Tahir, A. Rahimizadeh, J. Kalman, K. Fayazbakhsh, and L. Lessard, "Experimental and analytical investigation of 3D printed specimens reinforced by different forms of recyclates from wind turbine waste," *Polymer Composites*, vol. 42, no. 9, pp. 4533-4548, 2021, doi: 10.1002/pc.26166.